THE JOURNAL OF PHYSICAL CHEMISTRY B

Article

pubs.acs.org/JPCB

Suppression of $NaNO_3$ Crystal Nucleation by Glycerol: Micro-Raman Observation on the Efflorescence Process of Mixed Glycerol/$NaNO_3$/Water Droplets

Jun-Ying Yu,[†] Yun Zhang,[†] Guang Zeng,[†] Chuan-Ming Zheng,[†] Yong Liu,*[,‡] and Yun-Hong Zhang*[,†]

[†]The Institute of Chemical Physics, Key Laboratory of Cluster Science, School of Chemistry, Beijing Institute of Technology, Beijing 100081, People's Republic of China

[‡]Department of Chemistry, University of Colorado-Denver, Denver, Colorado 80217, United States

Supporting Information

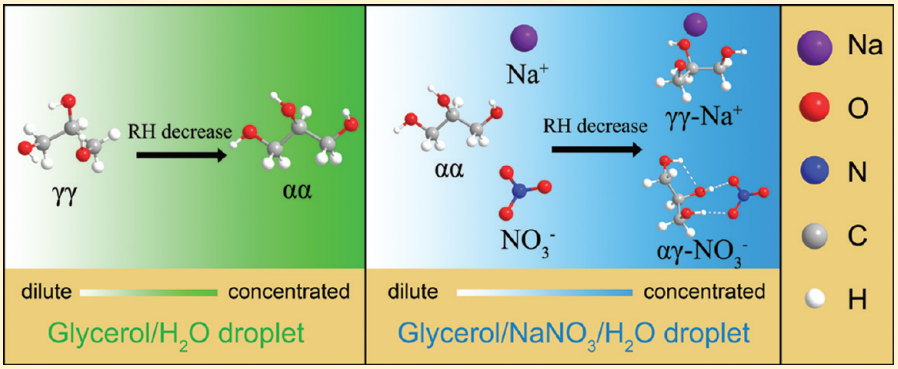

ABSTRACT: Although the hygroscopicity of a $NaNO_3$/water microdroplet and a polyalcohol/water microdroplet, two of the most important aerosols in atmosphere, has been widely studied, little is known about the relationship between the hygroscopic behavior of mixed $NaNO_3$/polyalcohol/water droplets and their structures on the molecular level. In this study, the hygroscopicity of mixed glycerol/$NaNO_3$/water droplets deposited on a hydrophobic substrate was studied by micro-Raman spectroscopy with organic-to-inorganic molar ratios (OIRs) of 0.5, 1, and 2. In the mixed glycerol/$NaNO_3$/water droplets, glycerol molecules tended to combine with Na^+ and NO_3^- ions by electrostatic interaction and hydrogen bonding, respectively. On the basis of the analyses of the changes of symmetric stretching (ν_s-CH_2), asymmetric stretching (ν_a-CH_2), their area ratio ($A\nu_a$-CH_2/$A\nu_s$-CH_2) of glycerol, and symmetric stretching band of NO_3^- (ν_1-NO_3^-) with relative humidity (RH), it was found that the conformation of glycerol was transformed from $\alpha\alpha$ mainly to $\gamma\gamma$ and partly to $\alpha\gamma$ with a decreasing RH in the mixed droplets, contrary to the case in the glycerol/water droplet. In addition, the glycerol with $\gamma\gamma$ and $\alpha\gamma$ conformation had strong interaction with Na^+ and NO_3^- respectively, which suppressed the formation of contact of ions and delayed the efflorescence relative humidity (ERH) for the mixed droplets compared to the $NaNO_3$/water droplet.

INTRODUCTION

Composition of atmospheric aerosols is very complicated because, besides inorganic compounds such as NaCl, $NaNO_3$, $(NH_4)_2SO_4$, $MgSO_4$, and $CaCO_3$, there are many organic species (fatty acids, alcohols, esters, hydrocarbons, etc.). These organics are largely originated from fossil fuel combustion, biogenic emission, and subsequent oxidation of gaseous precursors through which volatile organic compounds (VOCs) are transformed into low vapor pressure species. The less volatile species then generate secondary organic aerosols (SOAs) via nucleation or simple deposition onto pre-existing seeds. Organic aerosols can also be directly emitted to the atmosphere from biomass burning, to the ocean surface from marine autotrophic organism activity, through microbial emission from biosphere, cooking emission, or application of pesticides in agriculture operation.[1−6] Atmospheric organics are ubiquitous and abundant and generally account for 20−60% of total aerosol mass depending on local environments.[7,8] They can greatly affect the size distribution, hygroscopic behaviors, as well as radiation properties of atmospheric aerosols, hence impacting the Earth's climate system.

Hygroscopicity is one of the most fundamental properties of atmospheric aerosols. In the atmosphere, many aerosol particles with soluble inorganic components show properties of deliquescence, efflorescence, and hygroscopic growth. Like inorganic aerosols, atmospheric organics may also present such interesting properties in the humidifying/dehumidifying processes. Chan et al. studied the hygroscopic properties of amino acids,[9] dicarboxylic and multifunctional acids,[10] and water-soluble organic compounds

Received: November 10, 2011
Revised: January 5, 2012
Published: January 9, 2012

   dx.doi.org/10.1021/jp210824e | J. Phys. Chem. B 2012, 116, 1642−1650

(WSOCs) and their mixtures,[11] and concluded that only some atmospheric organics had deliquescence and efflorescence relative humidities (DRH and ERH), and their hygroscopic behaviors in multicomponent solutions were fairly different from those in individual aqueous solution.

Due to the potential climatic impacts of atmospheric organic species, recently there has been growing interest in the effects of organics on the hygroscopicity and phase transition of inorganic aerosol. Chan and co-workers[12] applied electrodynamic balance (EDB) technique to study the effects of glycerol, succinic acid, malonic acid, citric acid, and glutaric acid on the hygroscopic behaviors of sodium chloride (NaCl) and ammonium sulfate ($(NH_4)_2SO_4$) and found that the NaCl/water droplet was more sensitive to organics compared to $(NH_4)_2SO_4$. Reid's group[13−15] explored inorganic/organic mixtures with optical tweezers and Raman spectroscopy and revealed that an insoluble organic layer was formed on the surface of inorganic droplets. Ciobanu et al.[16] investigated a ternary system containing poly(ethylene glycol)-400/$(NH_4)_2SO_4$ in water, and concluded that the physical state of the mixture was dependent on the organic-to-inorganic ratio (OIR). Pandis et al.[17] probed the deliquescent behavior of mixed organic/inorganic droplets by measuring their size with increasing relative humidities (RHs) and found that pinonic acid/glutaric acid did not affect the DRH of NaCl and $(NH_4)_2SO_4$. Similar results were also reported by Marcolli et al.[18] In addition, Marcolli et al.[18,19] observed that the presence of organics in aerosol inhibited efflorescence of inorganic compounds. Despite great efforts devoted to the hygroscopicity of mixed organic/inorganic aerosols, at present, our knowledge at the molecular level about the interaction between organics and inorganics in the mixed droplets is still very limited.

Sea salt aerosols, generated by wind-induced wave action and bubble bursting of seawater, are the second largest component (by mass) of global aerosol burden.[20−22] While entrained in the atmosphere, these aerosols may undergo chemical processing via heterogeneous reactions with trace species in the atmosphere such as OH, O_3, HNO_3, NO_2, SO_2, and N_2O_5. One important reaction is between sea salt aerosols and nitric acid, during which halides are converted to nitrate. There has been convincing evidence from laboratory and field studies showing the formation of nitrate in the processed sea salt aerosol.[23−26] As such, like NaCl, the hygroscopicity of the $NaNO_3$ particles/droplet have also been extensively studied.[27−30]

Glycerol, the simplest polyalcohol, has been widely used in food, pharmaceutical, and personal care industries and has been identified as one of the major WSOCs in atmospheric aerosols.[31,32] Under standard atmospheric conditions, it exists as a liquid with low vapor pressure (~0.4 kPa). Although glycerol is ready to capture water, it does not present ERH and DRH over the entire humidity range. In addition, a recent study also showed that glycerol/water can form supercooled liquid when RH drops to ~29%.[16]

In this work, micro-Raman technique was employed to study the hygroscopicity of a mixed $NaNO_3$/glycerol/water droplet as a model system for mixed organic/inorganic aerosols. The objective of the present study is to understand how glycerol affects the hygroscopicity of $NaNO_3$ on the molecular level, especially the formation mechanism of contact ion pairs between Na^+ and NO_3^- in glycerol−water solutions and heterogeneous and homogeneous nucleation of $NaNO_3$ crystals in the mixture, as well as $NaNO_3$ crystal growth in the present of glycerol. In situ spectra and morphology images of the droplets were acquired under various RH conditions. Changes in symmetric stretching (ν_s-CH_2), asymmetric stretching (ν_a-CH_2) and their area ratio ($A\nu_a$-CH_2/$A\nu_s$-CH_2) of glycerol in the mixed droplets were used to infer glycerol conformational transformation and its interaction with Na^+, NO_3^- and H_2O during the evaporation process. In addition, peak position and full width at half-maximum (FWHM) of the symmetric stretching band of NO_3^- (ν_1-NO_3^-) and ν-CH_2 in the mixed glycerol/$NaNO_3$/water droplets at various RHs offer insight into the effects of glycerol on the hygroscopicity of $NaNO_3$ droplets.

EXPERIMENTAL SECTION

Sample Preparation. $NaNO_3$ stock solution with known concentration was first prepared by dissolving $NaNO_3$ (AR: analytical grade) directly into triply distilled water (Barnstead EASY pureII). Mixed glycerol/$NaNO_3$ solutions with different molar ratios were obtained by adding designated amounts of glycerol (CP: chemical pure) into the $NaNO_3$ stock solution. All chemicals were used directly without further treatment. The molar ratios between glycerol and sodium nitrate, i.e., the OIRs, were 0.5, 1, and 2, respectively. A syringe was used to inject the mixed droplets onto a substrate fixed in a homemade chamber. The substrate consists of a piece of quartz slide covered by a hydrophobic polytetrafluoroethylene (PTFE) film. The chamber was sealed with a transparent PE film. Because the size of the droplets was on the micrometer scale and because of the hydrophobic nature of the substrate, the effect of gravity can be neglected.[33] Additionally, the deposited droplets can be assumed to be spherical, similar to the shape of real aerosol suspended in the atmosphere. The RH in the chamber was controlled by adjusting the relative flow rates of dry N_2 and moist N_2 saturated with water vapor, and monitored by a hygrometer (Centertek Center 310, RH ± 2.5%, ± 0.7 °C).

Apparatus and Conditions for the Measurements. The instrumental setup used in this study is same as the one in our previous reports, and details about the setup can be found elsewhere.[27,34] Briefly, it is divided into three main parts: an RH-controlling system coupled to a sample chamber, a confocal Raman spectrometer (Renishaw Invia) used to record the Raman spectra, and a microscope (Leica DMLM) attached to the Raman system for imaging during the efflorescence process. The schematic diagram of the experimental setup is shown in Figure 1.

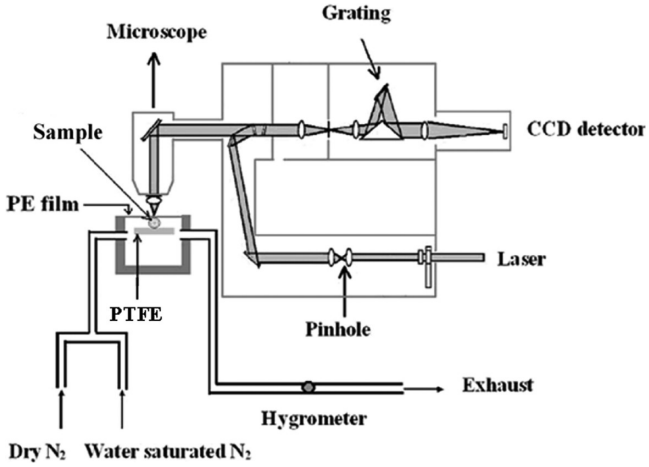

Figure 1. Schematic diagram of the experimental setup for the micro-Raman measurements of droplets on a PTFE substrate.

dx.doi.org/10.1021/jp210824e | J. Phys. Chem. B 2012, 116, 1642−1650

Micro-Raman spectra were recorded in the backscattering configuration with a 514.5 nm Ar^+ laser (LS-514 model, Laserphysics) as the excitation source. The output power was 20 mW. With a 50× objective lens, the laser beam was focused on the sample with a spot size of ~1 μm in diameter. The strong Rayleigh scattering was removed by a 514.5 nm notch filter. After passing through a 1800 g/mm grating, the dispersed Raman signals were then detected by a charge-coupled device (CCD). Spectral calibration was carried out with respect to a 520 cm^{-1} silicon band as the standard before each experiment. Raman spectra from 200 to 4000 cm^{-1} with 1 cm^{-1} resolution were obtained with three repeated scans, and each scan had an exposure time of 10 s. A droplet with size of ~40 μm was selected to be measured in each experiment. The droplet was blown for ~40 min at a given RH at a flow rate of 400 mL·min^{-1} to ensure that the droplet equilibrated with the ambient RH. The morphological changes during the efflorescence processes were observed through the microscope. All measurements were carried out at ambient temperature of 22–24 °C.

RESULTS AND DISCUSSION

Raman Spectra of a Mixed Glycerol/$NaNO_3$/Water Droplet at Different RHs. In our previous work, the efflorescence/deliquescence processes of individual $NaNO_3$ particles on a hydrophilic quartz substrate were observed by using Raman spectroscopy.[27] The droplets were usually hemispheres with large solid–liquid interfaces between the droplets and the hydrophilic quartz substrate, which were quite different from levitated aerosol droplets. In this study, droplets were deposited on a quartz slide covered with a piece of hydrophobic PTFE film. The $NaNO_3$/water and mixed glycerol/$NaNO_3$/water droplets on the PTEE film had little interface with the substrate. As a result, the effect of gravity on the microdroplet can be neglected,[33] and the shape of the droplets was nearly spherical, in resemblance to that of airborne atmospheric aerosol.

Figure 2 shows the Raman spectra of a $NaNO_3$/water droplet and the mixed glycerol/$NaNO_3$/water droplets with OIRs of 0.5, 1, and 2 at different RHs in dehumidifying processes. The morphological images of the droplets at various RHs are shown on the right side of the figure. The initial diameters were all about 40 μm in diameter.

For the $NaNO_3$/water droplet, as shown in the Figure 2a, the ν_1-NO_3^- band has continuous blue-shift from 1049 to 1055 cm^{-1} with RH decreasing from 96 to 47%. The FWHM of the band also increases from 10.3 to 13.8 cm^{-1}. As the RH is lowered to ~46%, a strong band appears at ~1066 cm^{-1}, which corresponds to the ν_1-NO_3^- band of $NaNO_3$ crystal, indicating that the droplet undergoes phase transition and transforms into crystal at this RH. A big envelope at ~3490 cm^{-1} with a shoulder at ~3256 cm^{-1} corresponds to the ν-OH (H_2O) band. The intensity of the main peak and the shoulder decreases with RH, and the envelopes disappear with RH decreasing below 46%.

For the mixed glycerol/$NaNO_3$/water droplet with an OIR of 0.5 shown in Figure 2b, the ν_1-NO_3^- band blue-shifts from 1050 to 1052 cm^{-1} with a decrease in RH from 90 to 42%. When the RH arrives at ~36%, a strong band appears at ~1066 cm^{-1}, indicating the crystallization of $NaNO_3$ in the mixed droplet. However, a peak appeared at ~1047 cm^{-1}, indicating that there is a small amount of NO_3^- anions remaining in the liquid phase. This peak remains present even with further decreases in RH. Besides the ν-OH (H_2O) band at ~3470 and ~3256 cm^{-1}, an additional shoulder appears at ~3400 cm^{-1},

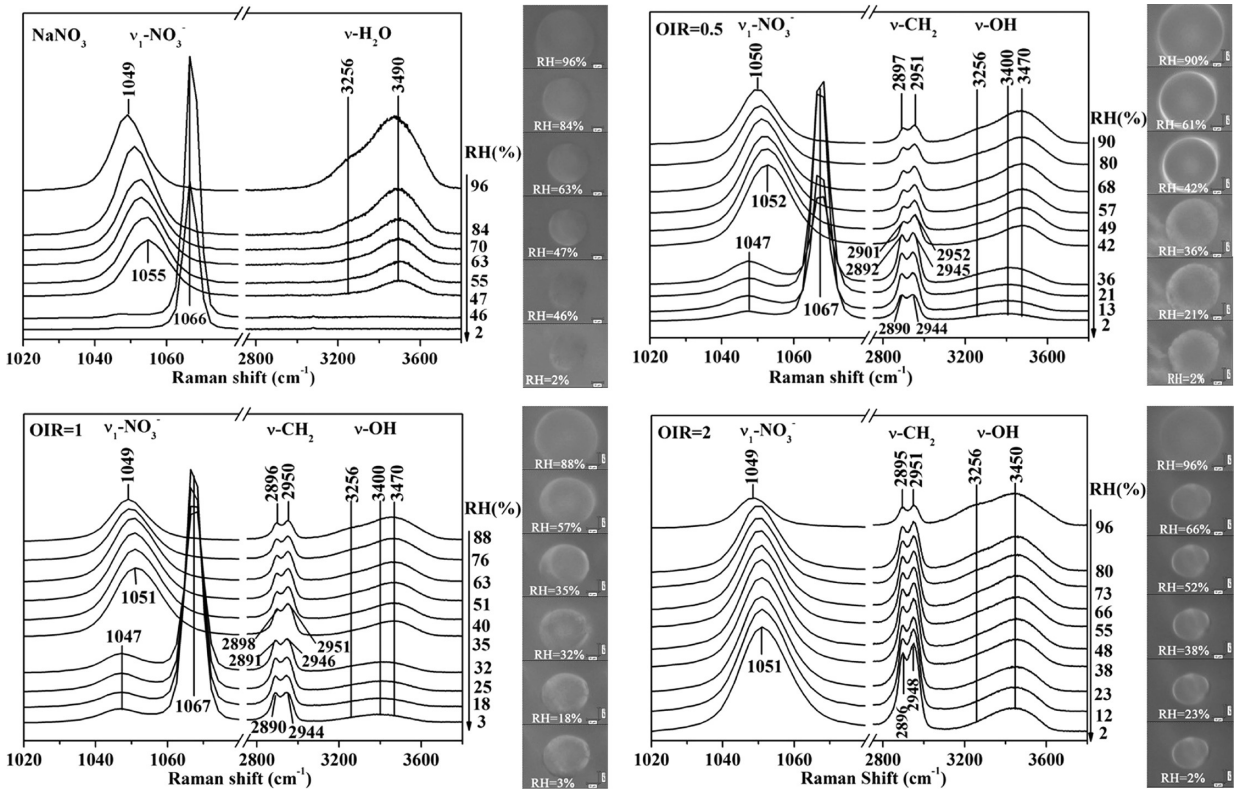

Figure 2. Raman spectra of the $NaNO_3$ droplet (a) and mixed glycerol/$NaNO_3$/water droplets with OIRs = 0.5 (b), 1 (c), and 2 (d) on PTFE substrate in dehumidifying processes. The pictures at the right side are the morphology of droplets at different RHs.

dx.doi.org/10.1021/jp210824e | J. Phys. Chem. B 2012, 116, 1642–1650

which is attributed to the ν-OH band of glycerol. The band at ~3400 cm^{-1} becomes the dominant peak after efflorescence. The ν-CH_2 bands blue-shift with RH decrease before efflorescence: from 2951 to 2952 cm^{-1} for the ν_a-CH_2 band, and from 2897 to 2901 cm^{-1} for the ν_s-CH_2 band. Red shifts of the ν-CH_2 bands occur abruptly at the point of ERH, i.e., ν_a-CH_2 to 2945 cm^{-1} and ν_s-CH_2 to 2892 cm^{-1}. The ν-CH_2 bands red-shift continuously with a further decrease in RH. The relative intensity between the ν_a-CH_2 band and the ν_s-CH_2 band is approximately equal to 1 at high RH (~90%) and increases simultaneously with a decrease in RH. The intensity increase in the ν_a-CH_2 band is higher than that of the ν_s-CH_2 band. After efflorescence, the intensities of the two bands are equal to each other again.

For the mixed glycerol/$NaNO_3$/water droplet with an OIR of 1 shown in Figure 2c, the ν_1-NO_3^- band blue-shifts from 1049 to 1051 cm^{-1} with RH decreasing from 88 to 35%. The strong solid $NaNO_3$ band appears at ~1067 cm^{-1} after efflorescence. The ν_1-NO_3^- band in the liquid phase also appears at ~1047 cm^{-1} at the point of ERH (~32%) just like that with the OIR of 0.5. Further decrease in RHs results in a small red-shift of the ν_1-NO_3^- band. The change of the ν-OH band is similar to that with the OIR of 0.5. The ν-CH_2 band blue-shifts with the decrease of RH before efflorescence: from 2950 to 2951 cm^{-1} for the ν_a-CH_2 band, and from 2896 to 2898 cm^{-1} for the ν_s-CH_2 band. Red shifts of the ν-CH_2 bands also occur abruptly at the point of ERH: the ν_a-CH_2 band to 2946 cm^{-1}, and the ν_s-CH_2 band to 2891 cm^{-1}. The change in the relative intensity between the ν_a-CH_2 band and the ν_s-CH_2 band with RH is similar to that of the droplet with the OIR of 0.5.

The droplet does not effloresce even at very low RH (~2%) for the mixed glycerol/$NaNO_3$/water droplet with an OIR of 2, as shown in Figure 2d. The ν_1-NO_3^- band blue-shifts from 1049 to 1051 cm^{-1} in the whole RH range from 96 to 2%. Because there is a large portion of glycerol in the mixed droplet with the OIR of 2, the OH stretching band is dominated by glycerol molecules instead of water. The ν–OH band shows a main peak at 3450 cm^{-1} with a shoulder at 3256 cm^{-1}, and the intensity of the shoulder decreases with decreasing RHs. The shifts of the ν-CH_2 bands are inhibited compared with those of the droplets with OIRs of 0.5 and 1. In the whole RH range from 96 to 2%, the ν_s-CH_2 band blue-shifts only 1 cm^{-1} from 2895 to 2896 cm^{-1}, while the ν_a-CH_2 band red-shifts 3 cm^{-1} from 2951 cm^{-1} to 2948 cm^{-1}. The change in the relative intensity between the ν_a-CH_2 band and the ν_s-CH_2 band with RH for the droplet with OIR = 2 is similar to those of droplets with OIR = 0.5 and 1.

The structure of glycerol molecule is flexible and has several different conformers ($\alpha\alpha$, $\beta\beta$, $\gamma\gamma$, $\alpha\beta$, $\alpha\gamma$, $\beta\gamma$) in crystal, liquid and glass states,[35] dependent on the changes in hydrogen bonds in the surrounding environment. The peak positions of the symmetric (ν_s-CH_2) and the asymmetric (ν_a-CH_2) stretching bands of CH_2 as well as the area ratio of ν_a-CH_2 to ν_s-CH_2 are usually used as criteria to judge the conformational structure of a glycerol molecule.[36−39] In this work, the Raman spectra of the glycerol/water droplet were also measured and compared with those of the mixed glycerol/$NaNO_3$/water droplets in the decreasing RH process, which offers information on the effect of $NaNO_3$ on the glycerol conformation in water.

The Conformer and Aggregation of Glycerol Molecules in Mixed Droplets. All covalent bonds in a glycerol molecule are single and can rotate freely to some degree. In addition, strong hydrogen bonds including intramolecule and intermolecule interactions exist extensively in liquid glycerol and glycerol aqueous solutions. As such, glycerol molecules can have several conformations according to their states. Riccardo Chelli obtained six different backbone structures ($\alpha\alpha$, $\alpha\beta$, $\alpha\gamma$, $\beta\beta$, $\beta\gamma$, $\gamma\gamma$) based on density functional calculation and experimental studies.[35,40,41] They also found that the $\alpha\alpha$ conformations predominate (~74%) in the liquid phase and $\gamma\gamma$ and $\alpha\gamma$ conformations account for ~19% and ~7%, respectively.

The hygroscopicity of glycerol and its effects on the hygroscopicity of inorganic salt aerosol have been studied by many groups.[11,12,42] In the pure state, glycerol molecules tend to self-aggregate by intermolecular hydrogen bonds and exist as open and cyclic dimers, trimers, and oligomers but not the linear chains.[29,43,44] However, for glycerol/water solutions, since water−glycerol hydrogen bonds would form at the expense of glycerol−glycerol intermolecular hydrogen bonds, the degree of glycerol aggregate diminishes, and glycerol molecules tend to form dimers and monomers upon dilution.[45] In glycerol aqueous solutions, H-bond interactions occur extensively between water/glycerol, water/water, and glycerol/glycerol molecules. The interior structure of the glycerol/water droplets is largely determined by the fraction of glycerol component, and it could become more complex with the addition of an inorganic compound, such as $NaNO_3$.

As glycerol has low volatility (p = 0.4 kPa, 20 °C), the relative concentration of glycerol to $NaNO_3$ is expected to remain unchanged in the three mixed solutions. However, thed ratio of ν_1-NO_3^- band area to ν-CH_2 band (sum of ν_a-CH_2 and ν_s-CH_2) area, i.e., Aν_1-NO_3^-/Aν-CH_2, increases slowly with decreasing RHs in the mixed glycerol/$NaNO_3$/water droplets with OIRs of 0.5, 1, and 2, which can be seen from Figure 3.

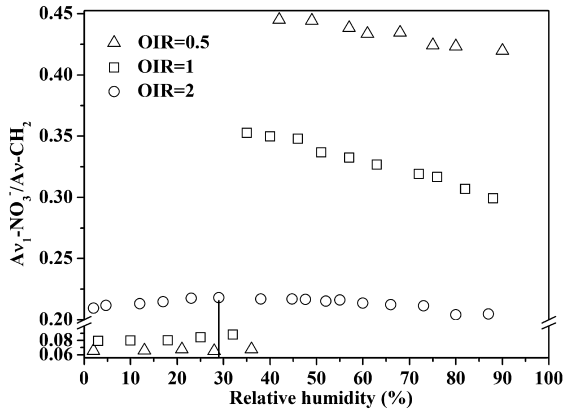

Figure 3. Area ratio of the ν_1-NO_3^- band to the ν-CH_2 band of the mixed glycerol/$NaNO_3$ droplets at various RHs in the efflorescence process.

Especially for the mixed droplet with OIR = 2, there is a peak for the Aν_1-NO_3^-/Aν-CH_2 curve at around RH = 28%. This may be caused by the formation of supercooled liquid at high concentration of glycerol[11,12] rather than glycerol volatilization. In addition, there is a sharp decrease in the Aν_1-NO_3^-/Aν-CH_2 curve when $NaNO_3$ crystallizes in the mixed droplets with OIRs of 0.5 and 1.

The area ratio of the ν_a-CH_2 band to the ν_s-CH_2 band is often used to evaluate the molecular conformation.[36−39] The symmetric stretching (ν_s-CH_2) and asymmetric stretching (ν_a-CH_2) are sensitive to molecular structure and ambient condition. The stretching of CH_2

dx.doi.org/10.1021/jp210824e | J. Phys. Chem. B 2012, 116, 1642−1650

in glycerol molecules with regular $\alpha\alpha$ conformation was observed at lower wavenumber than those with $\gamma\gamma$ conformation.[46,47]

Figure 4 shows the ratio of $A\nu_a$-CH_2/$A\nu_s$-CH_2 at various RHs for the glycerol/water droplet and the mixed glycerol/$NaNO_3$/

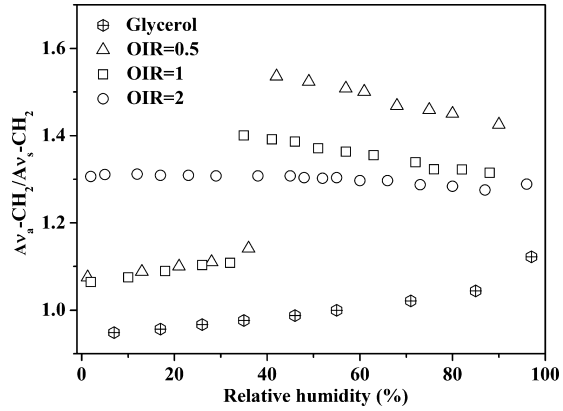

Figure 4. Area ratio of the ν_a-CH_2 band to the ν_s-CH_2 band of the glycerol/water droplet and the mixed glycerol/$NaNO_3$ droplets at various RHs in the dehumidifying process.

water droplets. Figure 5 presents the peak positions of the ν_a-CH_2 band and the ν_s-CH_2 band.

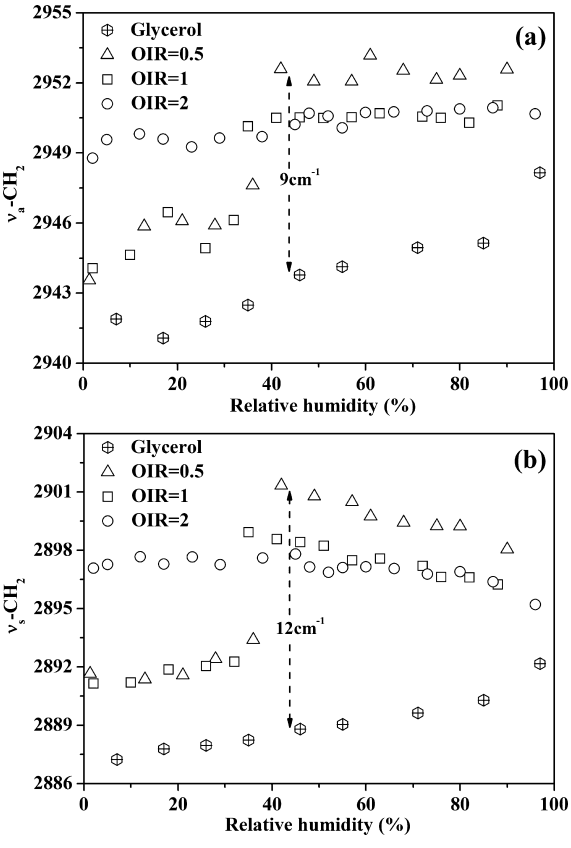

Figure 5. Raman shift of the ν_a-CH_2 band and the ν_s-CH_2 band of the glycerol/water droplets and the mixed glycerol/$NaNO_3$ droplets at various RHs in the dehumidifying process.

For the glycerol/water droplet, the ratio of $A\nu_a$-CH_2/$A\nu_s$-CH_2 in Figure 4 decreases with decreasing RHs, and this may indicate that the molecular structure tends to become more regular. Some glycerol molecules transform from the conformation of $\gamma\gamma$ into $\alpha\alpha$ with reducing perturbation of water molecules in the water evaporation process,[36] which is demonstrated in Scheme 1.

Scheme 1. Conformational Transformation of Glycerol Molecules between $\alpha\alpha$ and $\gamma\gamma/\alpha\gamma$

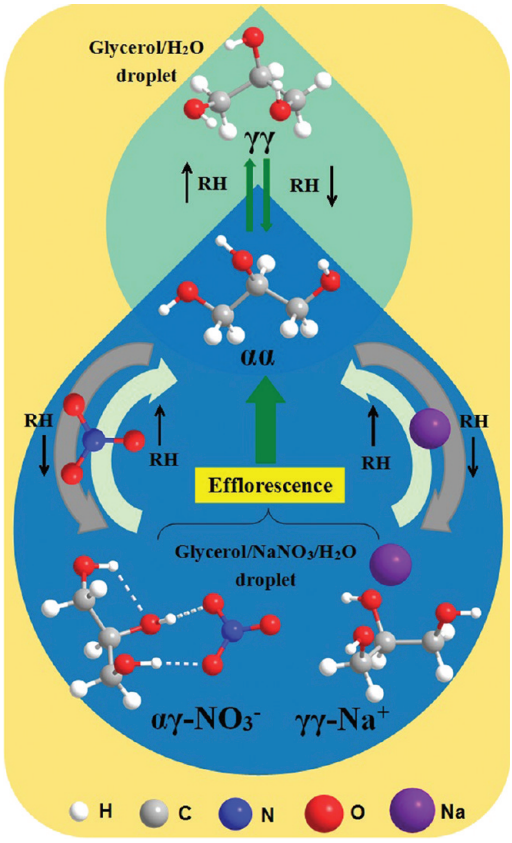

In Figure 5, both the ν_a-CH_2 band and the ν_s-CH_2 band in the glycerol/water red-shift during evaporation, which confirms that molecular conformation tends to possess the more regular $\alpha\alpha$.[46] The reason is that, without the perturbation of hydrogen bonds from water molecules, the $\alpha\alpha$ glycerol molecules are more stable, which can self-aggregate to the open and cyclic dimers, trimers, and oligomers by intermolecular hydrogen bonds.

For the mixed glycerol/$NaNO_3$/water droplets, the $A\nu_a$-CH_2/$A\nu_s$-CH_2 ratios in Figure 4 as a function of RH during the evaporation process are drastically different from that of the glycerol/water droplet, as well as the shift of the ν-CH_2 bands in Figure 5. The ratios of $A\nu_a$-CH_2/$A\nu_s$-CH_2 of the mixed glycerol/$NaNO_3$/water droplets with OIRs of 0.5, 1, and 2 increase with decreasing RHs before efflorescence and are much higher than that of the glycerol/water droplet in the same RH range. The increase in the ratio is enhanced by the additional amount of $NaNO_3$ in the mixed droplets. At the ERHs of the mixed droplets with OIRs of 0.5 and 1, the ratios of $A\nu_a$-CH_2/$A\nu_s$-CH_2 drop abruptly and decrease with further decrease in RHs. In Figure 5, both the ν_a-CH_2 band and the ν_s-CH_2 band of the mixed droplets are much higher than those of the glycerol/water droplet in the same RH range. The degrees of the blue-shift of the ν-CH_2 bands are enhanced by the additional amount of $NaNO_3$ in the mixed droplets. The largest blue-shifts for the ν_a-CH_2 band and the ν_s-CH_2 band in OIR = 0.5 droplets compared with the glycerol/water droplet at RH 45% are ~9 and ~12 cm^{-1}, respectively. With decreasing RHs, the ν_s-CH_2 band

dx.doi.org/10.1021/jp210824e | J. Phys. Chem. B 2012, 116, 1642–1650

slightly shifts to higher wavenumber before efflorescence, while the ν_a-CH_2 band remains constant. After efflorescence, the ν_s-CH_2 band red-shifts from 2901 to 2893 cm^{-1} for the mixed droplet with an OIR of 0.5 and from 2899 to 2892 cm^{-1} for that with an OIR of 1, while the ν_a-CH_2 band shifts from 2952 to 2947 cm^{-1} for OIR = 0.5 and from 2950 cm^{-1} to 2946 cm^{-1} for OIR = 1.

As discussed above, water-free glycerol molecules tend to form aggregates with $\alpha\alpha$ conformation as the dominant component. Water molecules can form hydrogen bonds with glycerol molecules and convert some $\alpha\alpha$ conformation into $\gamma\gamma$ ones, resulting in an increase in the ratio of $A\nu_a$-CH_2/$A\nu_s$-CH_2 and a blue-shift of the ν_a-CH_2 and ν_s-CH_2 bands as RH increases. According to results from density functional theory (DFT) calculation at the B3-LYP/6-31G(d, p) level, with the addition of $NaNO_3$, Na^+ and NO_3^- would interact with glycerol molecules through electrostatic or hydrogen-bonding interactions. Table 1 shows the energies of the complex isomers

Table 1. Calculated Energies of Isomers of the Complexes between Glycerol and Na^+ and NO_3^-

		Na^+···glycerol		NO_3^-···glycerol	
conformer	E_{DFT} (a.u.)	E_{DFT} (a.u.)	ΔE_{DFT} (kJ/mol)	E_{DFT} (a.u.)	ΔE_{DFT} (kJ/mol)
$\alpha\alpha$	−344.816 962 08	−506.969 668 93	0	−625.237 727 79	0
$\gamma\gamma$	−344.818 347 68	−506.976 519 80	−17.995	−625.236 488 66	3.255
				−625.232 374 79	14.061
$\alpha\gamma$	−344.810 708 95	−506.969 062 38	1.593	−625.237 456 91	0.712
		−506.966 931 53	7.190	−625.238 278 28	−1.446

calculated by DFT at the B3-LYP/6-31G(d, p) level. One glycerol molecule with $\gamma\gamma$ conformation has the advantage of forming a $\gamma\gamma$−Na^+ complex with a tetrahedron structure in space through three hydroxyl O atoms of the $\gamma\gamma$ glycerol with one Na^+ by electrostatic interaction, as shown in Scheme 1. The $\gamma\gamma$−Na^+ complex has one stable closed six-membered ring (−C2−C1−O···Na^+···O−C3−) and two stable closed five-membered rings (−C1−O···Na^+···O−C2− and −C2−O···Na^+···O−C3−), of which the energy is about 18.0 kJ·mol^{-1} lower that of the $\alpha\alpha$−Na^+ complex having only one five-membered ring (−C1−O···Na^+···O−C2−). Meanwhile, glycerol molecules with $\alpha\gamma$ conformation could form the most stable complex ($\alpha\gamma$- NO_3^-) with NO_3^- ions through hydrogen-bonds as hydrogen donors according to Table 1. Thus, a large increase of the $A\nu_a$-CH_2/$A\nu_s$-CH_2 ratio and efficient blue shift of the ν_a-CH_2 and ν_s-CH_2 bands in the mixed glycerol/$NaNO_3$/water droplets with OIRs of 0.5 and 1 compared to the glycerol/water droplet at the same RHs indicate that $\alpha\alpha$ conformation transforms into $\gamma\gamma$ or $\alpha\gamma$ conformation for the additional $NaNO_3$. Continuous increases in the ratio and blue-shifting of the bands with decreasing RHs reveal enhanced interactions of Na^+ and NO_3^-, which induces more $\alpha\alpha$ conformation conversion into mainly $\gamma\gamma$ and partly $\alpha\gamma$ conformation.

After efflorescence, some glycerol molecules with $\gamma\gamma$ conformation transform to $\alpha\alpha$ conformation because of crystallization of $NaNO_3$ and loss of water in the mixed droplets with OIRs of 0.5 and 1. Some Na^+ and NO_3^- are still dissolved in glycerol, which leads to the higher value of $A\nu_a$-CH_2/$A\nu_s$-CH_2 and blue shift of the ν-CH_2 bands compared to the glycerol/water droplet when RHs are lowered below $NaNO_3$ ERHs.

Because of predominant amount of glycerol in the mixed droplet with an OIR of 2, almost all Na^+ and NO_3^- ions interact with glycerol molecules in $\gamma\gamma$ conformation rather than water. As a result, transformation of glycerol's conformation is nearly unnoticeable throughout the whole RH. This is demonstrated by the curves of $A\nu_a$-CH_2/$A\nu_s$-CH_2 and the shifts of ν-CH_2 as a function of RH in Figures 4 and 5.

The Effect of Additional Glycerol on the Hygroscopicity of the $NaNO_3$ Droplet. In bulk $NaNO_3$ solutions and droplets, ion pairs between Na^+ and NO_3^- were revealed with the Raman spectroscopic technique.[27,48] Width and frequency of the ν_1-NO_3^- band were found to be sensitive to the ion pair structure.[48] According to the analysis of the Raman spectra of $NaNO_3$ droplets, the structure of NO_3^- anions transformed among free solvated nitrate ions, solvent-separated ion pairs (SIPs), contact ion pairs (CIPs), and complex ion aggregates with ambient RHs decreased from 82.0 to 29.5%.[27] The blue shifting and broadening of the ν_1-NO_3^- band were assigned to the transformation of NO_3^- anions from the free solvated ions (1047.6 cm^{-1} with bandwidth of 3.40 cm^{-1}) to SIPs (1049.0 cm^{-1} and 3.55 cm^{-1}), CIPs (1052.5 cm^{-1}, 8.11 cm^{-1}), and complex ion aggregates. The addition of glycerol could affect the formation and transformation of ion pairs in $NaNO_3$/water droplets.

The influence of glycerol on $NaNO_3$ was observed to be different from that on NaCl and $(NH_4)_2SO_4$ in previous work.[12] In this work, the $NaNO_3$/water droplets with an initial diameter of ~40 μm effloresced at 47−53%, as seen in Figure 2a. Under the same experimental conditions, including droplet size, humidity, and temperature, the ERHs of the mixed glycerol/$NaNO_3$/water droplets with different OIRs were found to be lower than that of $NaNO_3$/water droplets. The ERH with an OIR of 0.5 was located at 36−42%. When the OIR was equal to 1, the ERH dropped to 20−36%. The phase transformation of the mixed droplets from liquid to solid became more and more difficult with increasing OIR. The mixed glycerol/$NaNO_3$/water droplets with an OIR of 2 did not crystallize even at very low RH (~2%) as shown in Figure 2d. This can be attributed to the extra amount of glycerol in the mixture, which effectively suppressed the efflorescence. Such phenomena was also observed by Marcoll's group and is believed to account for the fact that some atmospheric aerosols exist in liquid phase even under very low RH conditions.[18,19]

Figure 6 shows the peak positions of the ν_1-NO_3^- band of the $NaNO_3$/water droplet and the mixed glycerol/$NaNO_3$/water droplets as a function of RH. The ν_1-NO_3^- bands of all the droplets blue-shift before efflorescence with decreasing RHs, but degrees of the blue-shift are decreased by the extra glycerol in the mixed droplets. For the $NaNO_3$/water droplet, the ν_1-NO_3^- band has a blue-shift of 6 cm^{-1} from 1049 to 1055 cm^{-1} as RH decreased from 96 to 47%. For the mixed glycerol/$NaNO_3$/water droplet with an OIR of 0.5, the ν_1-NO_3^- band blue-shifts only 2 cm^{-1} in the RH range between 90% and 42%. In the RH range of 88% to 35%, the ν_1-NO_3^- band blue-shifts just 2 cm^{-1} for the mixed droplet with an OIR of 1. While for the mixed droplet with an OIR of 2, it does not crystallize even at very low RH (~2%) for an extended period of time, and the ν_1-NO_3^- band blue shifts only 2 cm^{-1} from 1049 to 1051 cm^{-1} in the whole RH from 96 to 2%. The peak position of the ν_1-NO_3^- band in the mixed glycerol/$NaNO_3$/water droplets has a smaller wavenumber blue shift than that in $NaNO_3$/water

dx.doi.org/10.1021/jp210824e | J. Phys. Chem. B 2012, 116, 1642−1650

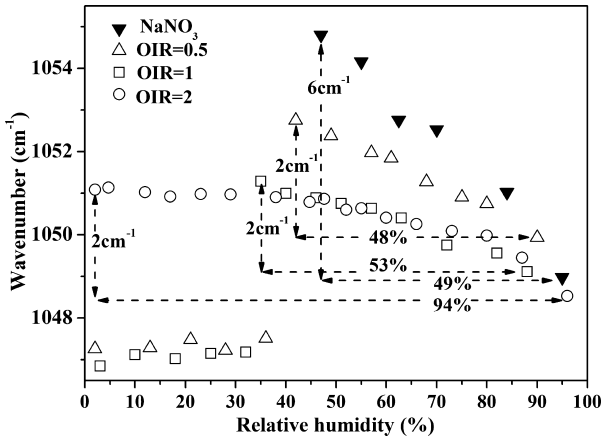

Figure 6. Raman shift of the ν_1-NO_3^- band of the mixed glycerol/$NaNO_3$ droplets at various RHs in the dehumidifying process.

droplet during the evaporation process. This indicates that the formation of ion pairs between Na^+ and NO_3^- is much easier in the $NaNO_3$/water droplet than in the mixed glycerol/$NaNO_3$/water droplets. The hydrations of Na^+ and NO_3^- in aqueous solutions have been studied commendably.[49,50] Scheme 1 shows the interactions between glycerol molecules and Na^+ and NO_3^- ions, as well as the structure of glycerol. In the mixed glycerol/$NaNO_3$/water droplets, in addition to hydration, a portion of Na^+ and NO_3^- ions interact with glycerol through electrostatic interaction and hydrogen-bonding, respectively. Additionally, the interactions become stronger with the loss of water before the ERH for the droplets with OIRs of 0.5 and 1 and in the whole RH range for the droplet with an OIR of 2. This hinders the direct contact between Na^+ and NO_3^-. Furthermore, glycerol molecules are larger and more flexible than water molecules. The steric effect in glycerol molecules inhibits the formation of CIPs between Na^+ and NO_3^- in the mixed droplets. Formation of the CIPs is directly related to the possibility of homogeneous nucleation in the supersaturated droplets. Therefore the addition of glycerol in $NaNO_3$ droplets is able to suppress the formation of CIPs, hence delaying efflorescence as observed in the present work.

After efflorescence, the symmetric stretching band of NO_3^- ions (ν_1-NO_3^-) still exists and red-shifts to 1047 cm^{-1} (Figure 6) for the mixed glycerol/$NaNO_3$/water droplets with OIR = 0.5 and 1. This case cannot occur in the $NaNO_3$/water droplet. This is because some $NaNO_3$ is still dissolved in the glycerol droplets, which is consistent with the aforementioned conclusion.

Figure 7 shows FWHMs of the ν_1-NO_3^- band as a function of RH for the $NaNO_3$/water droplet and the mixed glycerol/$NaNO_3$/water droplets. Before efflorescence, the ν_1-NO_3^- bands of all droplets broaden continuously with a decrease in RH for the formation of Na^+–NO_3^- ion pairs. In the whole RH range before efflorescence, the FWHMs of the ν_1–NO_3^- band for the mixed droplets are larger than that of the $NaNO_3$/water droplet. After efflorescence, the width of the ν_1-NO_3^- band becomes sharply narrow for the mixed droplets with OIRs of 1 and 0.5.

The FWHM is related to the NO_3^- structural multiplicity and their distribution in the droplets. In the $NaNO_3$/water droplet, it is largely determined by the formation of different ion pairs, including SIPs, CIPS, and complex CIPs. In the mixed droplets, interaction between glycerol and NO_3^- through hydrogen bonding could result in new kinds of complexes of glycerol–NO_3^-, which affects the FWHM. After efflorescence, residual

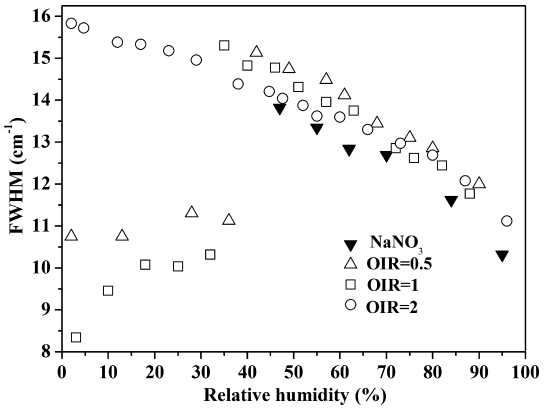

Figure 7. The FWHM of the ν_1-NO_3^- band of the mixed glycerol/$NaNO_3$ droplets at various RHs in the dehumidifying process.

Na^+ and NO_3^- in the mixed glycerol/$NaNO_3$/water droplets with OIR 0.5 and 1 could exist in the form of glycerol–Na^+ and glycerol–NO_3^- complexes and have lower possibility to form ion pairs, which sharply reduces the width of the ν_1-NO_3^- band.

The Characteristics of the Mixed Micro-Sized Particle after Efflorescence. The mixed droplet with an OIR of 2 does not crystallize even at very low RH (~2%). Considering that two glycerol molecules can provide Na^+ with six oxygen atoms to form a complex of $Na^+(glycerol)_2$, and the mixed droplet with an OIR of 2 happens to meet the stoichiometric requirement,[51] this could suppress the formation of CIPs and thus result in no ERH observed for the mixed droplet with an OIR of 2. For the mixed glycerol/$NaNO_3$/water particles with OIRs of 0.5 and 1, the ν_1-NO_3^- band shifts to lower frequency (~1047 cm^{-1}) after efflorescence, indicating that some NO_3^- ions still exist in the glycerol droplets even at very low RH (2% and 3%) with the formation of glycerol–Na^+ and glycerol–NO_3^- complexes (see Figure 6 and Scheme 1).

Interestingly, it is found that OIR also affects the size of $NaNO_3$ crystals in the mixed particles. Figure 8 shows the

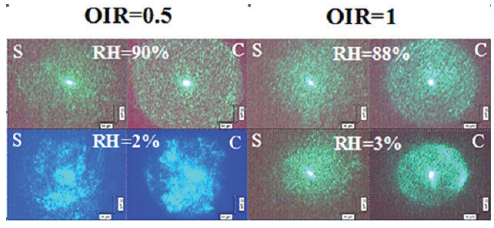

Figure 8. Laser images focused on the surface and in the center of the mixed glycerol/$NaNO_3$ droplets at various RHs in the dehumidifying process.

images of mixed glycerol/$NaNO_3$ droplets. For homogeneous droplets on the hydrophobic substrate, the laser beam can be well focused twice on the surface and on the center of the spherical droplets, respectively, as shown in images of the mixed droplets with an OIR of 0.5 at RH = 90% and an OIR of 1 at RH = 88%. After efflorescence, the mixed droplet with OIR = 0.5 at RH = 2% shows irregular strong scattering induced by different size $NaNO_3$ crystals in the droplets, and it is not possible to focus the laser on the center of the droplet again. For the mixed droplet with an OIR of 1 at RH = 3%, however, the twice focus can still be achieved, even though solid $NaNO_3$ crystallizes in the droplets. It means that the mixed droplet with an OIR of 1 after efflorescence

dx.doi.org/10.1021/jp210824e | J. Phys. Chem. B 2012, 116, 1642–1650

is a spherical solid−liquid mixed droplet, in which very small size $NaNO_3$ crystals are homogeneously distributed.

CONCLUSION

In the present work, we used micro-Raman technique to study the hygroscopic behaviors of a $NaNO_3$/water droplet and mixed glycerol/$NaNO_3$/water droplets on a hydrophobic substrate. The conformational transformation of glycerol molecules in the mixed droplets and the effects of glycerol on the hygroscopicity of the $NaNO_3$/water droplet during the efflorescence process were analyzed. Several interesting findings were obtained by analyzing the changes of the symmetric stretching of NO_3^- of $NaNO_3$ and the stretching of CH_2 bands of glycerol with decreasing RHs. In the mixed glycerol/$NaNO_3$/water droplets, water molecules, Na^+, and NO_3^- ions affected the structure of glycerol molecules. In the pure liquid glycerol, most glycerol molecules exist in stable $\alpha\alpha$ conformation, and they tend to self-aggregate to form open and cyclic dimers, trimers, and oligomers by intermolecular hydrogen bonds. In glycerol/water droplets, water molecules break the intermolecular hydrogen bonds between glycerol molecules, and the conformer of glycerol transforms from $\alpha\alpha$ to $\gamma\gamma$ with increasing RHs. The addition of $NaNO_3$ changes such conformational transformation of glycerol to the contrary in the mixed glycerol/$NaNO_3$/water droplets. This is because Na^+ and NO_3^- ions can be combined with glycerol molecules with $\gamma\gamma$ or $\alpha\gamma$ conformation by electrostatic interaction and hydrogen-bonding, promoting the conformer of glycerol transform from $\alpha\alpha$ to $\gamma\gamma$ or $\alpha\gamma$.

Glycerol affects the hygroscopicity of $NaNO_3$ by dilution, molecular steric effect, and interactions with ions, which suppress the formation of contact ions and in turn the efflorescence of $NaNO_3$ in the mixed droplets. The ERHs of $NaNO_3$ in the pure $NaNO_3$/water droplets and in the mixed aqueous droplets with OIRs of 0.5 and 1 are at 47−53%, 36−42%, and 20−36%, respectively. The mixed aqueous droplet with an OIR of 2 does not form crystal even at very low RH (2%) for an extended period of time. The morphologies of $NaNO_3$ crystals in the mixed glycerol/$NaNO_3$/water droplets after the efflorescence are different in the case of OIR = 0.5 and 1. Additionally, the crystal size is larger in the example with an OIR of 0.5 than that with an OIR of 1.

ASSOCIATED CONTENT

Supporting Information

Information about the optimized geometries of the complex isomers is available free of charge via the Internet at http://pubs.acs.org.

AUTHOR INFORMATION

Corresponding Author

*Telephone: 86-10-68913596; fax: 86-10-68912652; e-mail: yhz@bit.edu.cn (Y.-H.Z); yong.liu@ucdenver.edu (Y.L.).

ACKNOWLEDGMENTS

This work is supported by the NSFC (41175119, 20933001, and 20873006) and 111 project B07012. Yong Liu acknowledges the financial support from Research Corporation for Science Achievement.

REFERENCES

(1) Rudich, Y. *Chem. Rev.* **2003**, *103*, 5097−5124.
(2) Hoffmann, T.; O'Dowd, C. D.; Seinfeld, J. H. *Geophys. Res. Lett.* **2001**, *28*, 1949−1952.
(3) O'Dowd, C. D.; Jimenez, J. L.; Bahreini, R.; Flagan, R. C.; Seinfeld, J. H.; Hämeri, K.; Pirjola, L.; Kulmala, M.; Jennings, S. G.; Hoffmann, T. *Nature* **2002**, *417*, 632−636.
(4) Kalberer, M.; Paulsen, D.; Sax, M.; Steinbacher, M.; Dommen, J.; Prevot, A. S. H.; Fisseha, R.; Weingartner, E.; Frankevich, V.; Zenobi, R.; et al. *Science* **2004**, *303*, 1659−1662.
(5) Koehler, C. A.; Fillo, J. D.; Ries, K. A.; Sanchez, J. T.; De Haan, D. O. *Environ. Sci. Technol.* **2004**, *38*, 5064−5072.
(6) Kanakidou, M.; Seinfeld, J. H.; Pandis, S. N.; Barnes, I.; Dentener, F. J.; Facchini, M. C.; Van Dingenen, R.; Ervens, B.; Nenes, A.; Nielsen, C. J.; et al. *Atmos. Chem. Phys.* **2005**, *5*, 1053−1123.
(7) Duce, R. A.; Mohnen, V. A.; Zimmerman, P. R.; Grosjean, D.; Cautreels, W.; Chatfield, R.; Jaenicke, R.; Ogren, J. A.; Pellizzari, E. D.; Wallace, G. T. *Rev. Geophys. Space Phys.* **1983**, *21*, 921−952.
(8) Chow, J. C.; Watson, J. G.; Fujita, E. M.; Lu, Z. Q.; Lawson, D. R.; Ashbaugh, L. L. *Atmos. Environ.* **1994**, *28*, 2061−2080.
(9) Chan, M. N.; Choi, M. Y.; Ng, N. L.; Chan, C. K. *Environ. Sci. Technol.* **2005**, *39*, 1555−1562.
(10) Peng, C.; Chan, M. N.; Chan, C. K. *Environ. Sci. Technol.* **2001**, *35*, 4495−4501.
(11) Choi, M. Y.; Chan, C. K. *J. Phys. Chem. A* **2002**, *106*, 4566−4572.
(12) Choi, M. Y.; Chan, C. K. *Environ. Sci. Technol.* **2002**, *36*, 2422−2428.
(13) Buajarern, J.; Mitchem, L.; Reid, J. P. *J. Phys. Chem. A* **2007**, *111*, 9054−9061.
(14) Buajarern, J.; Mitchem, L.; Reid, J. P. *J. Phys. Chem. A* **2007**, *111*, 11852−11859.
(15) Buajarern, J.; Mitchem, L.; Reid, J. P. *J. Phys. Chem. A* **2007**, *111*, 13038−13045.
(16) Ciobanu, V. G.; Marcolli, C.; Krieger, U. K.; Weers, U.; Peter, Th. *J. Phys. Chem. A* **2009**, *113*, 10966−10978.
(17) Cruz, C. N.; Pandis, S. N. *Environ. Sci. Technol.* **2000**, *34*, 4313−4319.
(18) Marcolli, C.; Luo, B. P.; Peter, Th. *J. Phys. Chem. A* **2004**, *108*, 2216−2224.
(19) Marcolli, C.; Luo, B. P.; Peter, Th.; Wienhold, F. G. *Atmos. Chem. Phys.* **2004**, *4*, 2593−2599.
(20) Weis, D. D.; Ewing, G. E. *J. Geophys. Res.* **1999**, *104*, 21275−21285.
(21) Blanchard, D. C. *J. Geophys. Res.* **1985**, *90*, 961−963.
(22) Cipriano, R. J.; Blanchard, D. C. *J. Geophys. Res.* **1981**, *86*, 8085−8092.
(23) Gard, E. E.; Kleeman, M. J.; Gross, D. S.; Hughes, L. S.; Allen, J. O.; Morrical, B. D.; Fergenson, D. P.; Dienes, T.; Galli, M. E.; Johnson, R. J.; et al. *Science* **1998**, *279*, 1184−1187.
(24) Paerl, H. W. *Environ. Sci. Technol.* **2002**, *36* (15), 323A−326A.
(25) Gibson, E. R.; Hudson, P. K.; Grassion, V. H. *J. Phys. Chem. A* **2006**, *110*, 11785−11799.
(26) Saul, T. D.; Tolocka, M. P.; Johnston, M. V. *J. Phys. Chem. A* **2006**, *110*, 7614−7620.
(27) Li, X. H.; Wang, F.; Lu, P. D.; Dong, J. L.; Wang, L. Y.; Zhang, Y. H. *J. Phys. Chem. B* **2006**, *110*, 24993−24998.
(28) Lu, P. D.; Wang, F.; Zhao, L. J.; Li, W. X.; Li, X. H.; Dong, J. L.; Zhang, Y. H.; Lu, G. Q. *J. Chem. Phys.* **2008**, *129*, 104509.
(29) Liu, Y.; Yang, Z. W.; Desyaterik, Y.; Gassman, P. L.; Wang, H.; Laskin, A. *Anal. Chem.* **2008**, *80*, 633−642.
(30) Tang, I. N.; Munkelwitz, H. R. *J. Geophys. Res.* **1994**, *99*, 18801−18808.
(31) Zappoli, S.; Andracchio, A.; Fuzzi, S.; Facchini, M. C.; Gelencsér, A.; Kiss, G.; Krivácsy, Z.; Molnár, Á.; Mészáros, E.; Hansson, H. C.; et al. *Atmos. Environ.* **1999**, *33*, 2733−2743.
(32) Kawamura, K.; Ikushima, K. *Environ. Sci. Technol.* **1993**, *27*, 2227−2235.
(33) Khismatullin, D. B.; Nadim, A. *Phys. Rev. E* **2001**, *63*, 061508.
(34) Wang, F.; Zhang, Y. H.; Li, S. H.; Wang, L. Y.; Zhao, L. J. *Anal. Chem.* **2005**, *77*, 7148−7155.

(35) Chelli, R.; Gervasio, F. L.; Gellini, C.; Procacci, P.; Cardini, G.; Schettino, V. *J. Phys. Chem. A* **2000**, *104*, 5351−5357.
(36) Gaber, B. P.; Peticolas, W. L. *Biochim. Biophys. Acta, Biomembr.* **1977**, *465*, 260−274.
(37) Bunow, M. R.; Levin, I. W. *Biochim. Biophys. Acta, Lipids Lipid Metab.* **1977**, *487*, 388−394.
(38) Larsson, K.; Rand, R. P. *Biochim. Biophys. Acta, Lipids Lipid Metab.* **1973**, *326*, 245−255.
(39) Larsson, K. *Chem. Phys. Lipids* **1972**, *9*, 181−195.
(40) Chelli, R.; Procacci, P.; Cardini, G.; Califano, S. *Phys. Chem. Chem. Phys.* **1999**, *1*, 879−885.
(41) Chelli, R.; Procacci, P.; Cardini, G.; Della Valle, R. G.; Califano, S. *Phys. Chem. Chem. Phys.* **1999**, *1*, 871−877.
(42) Parsons, M. T.; Knopf, D. A.; Bertram, A. K. *J. Phys. Chem. A* **2004**, *108*, 11600−11608.
(43) Mendelovici, E.; Frost, R. L.; Kloprogge, T. *J. Raman. Spectrosc.* **2000**, *31*, 1121−1126.
(44) Padró, J. A.; Saiz, L.; Guàrdia, E. *J. Mol. Struct.* **1997**, *416*, 243−248.
(45) Mudalige, A.; Pemberton, J. E. *Vib. Spectrosc.* **2007**, *45*, 27−35.
(46) Tu, A. T. *Raman Spectroscopy in Biology: Principles and Applications*; Wiley: New York, 1982.
(47) Cheng, X. L.; Huo, L. H.; Gao, S.; Wang, H. S.; Wang, D. M.; Xi, S. Q. *Chin. J. Anal. Chem.* **2002**, *30*, 1330−1332.
(48) Frost, R. L.; James, D. W. *J. Chem. Soc., Faraday Trans. 1* **1982**, *78*, 3249−3261.
(49) Wang, X. B.; Yang, X.; Wang, L. S.; Nicholas, J. B. *J. Chem. Phys.* **2002**, *116* (2), 561−570.
(50) Caminiti, R.; Licheri, G.; Paschina, G.; Piccaluga, G.; Pinna, G. *J. Chem. Phys.* **1980**, *72* (8), 4522−4528.
(51) Mahoney, J. M.; Stucker, K. A.; Jiang, H.; Carmichael, I.; Brinkmann, N. R.; Beatty, A. M.; Noll, B. C.; Smith, B. D. *J. Am. Chem. Soc.* **2005**, *127*, 2922−2928.